High-bandwidth warm-atom quantum memory using hollow-core photonic crystal fibers

Jed Rowland,[1] Christopher Perrella,[1,2,*] Andre N. Luiten,[1] Rafal Gartman,[3] Krzysztof T. Kaczmarek,[3] Joshua Nunn,[3,4] and Ben M. Sparkes[1,5]

[1] *Institute for Photonics and Advanced Sensing (IPAS) and School of Physical Sciences, University of Adelaide, Adelaide, South Australia 5005, Australia*

[2] *Centre of Light for Life (CLL) and School of Biological Sciences, University of Adelaide, Adelaide, South Australia 5005, Australia*

[3] *ORCA Computing Ltd, London, United Kingdom*

[4] *CPPM University of Bath, Claverton Down, Bath BA27AY, United Kingdom*

[5] *Defence Science and Technology Group, Edinburgh, South Australia 5111, Australia*

(Received 26 October 2023; accepted 15 December 2023; published 24 January 2024)

We present an experimental realization of a noise-free and high-bandwidth quantum memory scheme using a rubidium vapor that is confined within the hollow core of a photonic crystal fiber. We achieve the same internal efficiencies as similar free-space experiments (30%) for 4.5-ns-long optical pulses but with a 100-fold reduction in the control-field power required. Modeling indicates that this efficiency could be improved to 88% with higher control powers and the implementation of techniques such as light-induced atomic desorption to increase the optical depth. The compactness, robustness, and low drive power of this approach lends itself to direct integration into large-scale fiber-based quantum processors.

DOI: 10.1103/PhysRevApplied.21.014048

I. INTRODUCTION

Optical approaches to quantum information operations offer a number of advantages over their matter-based counterparts [1,2]. For instance, light only weakly interacts with its environment, enabling guided-wave propagation with low loss without electrical or magnetic shielding. The high carrier frequency of optical signals enables room-temperature operation of quantum systems, removing the need for laser cooling or cryogenics. In addition, optical systems allow for high-bandwidth processing of quantum information and could make use of existing telecommunications components for future quantum computing networks [3]. The foremost problem facing the development of an optically based quantum computing system is the absence of on-demand entanglement when using linear optics [4–6]. It is therefore challenging to produce large multiphoton entangled states of light and the probability of producing these states falls exponentially with the number of photons needed.

One approach to solving this problem is to use quantum memories to synchronize probabilistic entangling operations in a repeat-until-success protocol [7]. The figures of merit by which a quantum memory are typically evaluated for such an application include the fidelity, efficiency, noise, lifetime, time-bandwidth product, and the practicality of the experimental setup [8,9]. The fidelity is the overlap between the recalled state and the input state, while the efficiency η_t is the percentage of the incident energy that can be retrieved from the memory at a specific time. Noise ν, determined from the fraction of recalled photons detected in the absence of a storage signal, will degrade the fidelity of the recalled information, even with a high efficiency. The lifetime τ_s is the time it takes for the efficiency to decrease by $1/e$ from its initial value due to decoherence inside the memory medium and is calculated from $\eta_{t=\tau_s} = \eta_0 e^{-1}$, where η_0 is the maximum memory efficiency. The bandwidth $\mathcal{B}$ is the rate at which operations can be performed, with larger bandwidths leading to faster computational clock rates as pulses with shorter temporal widths τ_p can be used.

The effective fractional delay combines the maximum efficiency, storage time, and pulse width $f_e = \eta_0 \tau_s / \tau_p$. The effective fractional delay is a key figure of merit for the synchronization of large multiphoton states in a repeat-until-success arrangement [7]. This is because, for a set storage time, the use of shorter pulses means that the system can be operated at a higher repetition rate and therefore increases the number of clock cycles over which the memory will allow for synchronization. Λ-type alkali vapor quantum memories are normally narrow band (megahertz) and have a fundamental bandwidth limitation of a few

*chris.perrella@adelaide.edu.au

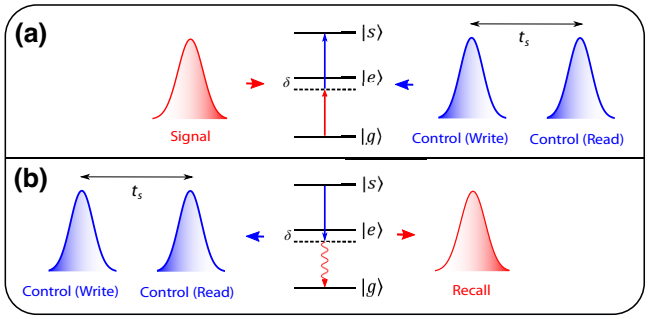

FIG. 1. The ORCA protocol. (a) The first "write" control pulse writes the signal into the storage medium, which has a ground state $|g\rangle$, an excited state $|e\rangle$, and a storage state $|s\rangle$, with a one-photon detuning δ from the excited state. (b) After a user-defined storage time t_s, a second "read" control pulse recalls the optical information from the memory.

gigahertz due to their ground-state splitting, significantly limiting the maximum f_e possible. This is unfortunate, as Λ-type memory protocols have achieved efficiencies over 90% [10], unconditional fidelities of 98% [11], and storage times of hundreds of milliseconds [12]. While broadband storage has been achieved at room temperature using Raman-type quantum memories [13–15]. All these Λ-type memories also suffer from inherent noise associated with the nonzero initial population of the storage state as well as four-wave-mixing noise [16]. Although this can be mitigated by optical pumping [13,17], it adds to the complexity of the system and sets some practical limitations.

Off-resonant cascaded absorption (ORCA) is a quantum memory protocol that offers a significantly improved fractional delay over other quantum memories, without the drawback of added noise, and can be implemented at room temperature [17–20]. Figure 1 shows the basics of the ORCA protocol operation. ORCA makes use of an atomic system with a three-level ladder energy structure consisting of a ground state, an excited state, and a storage state. A signal field and a control field undergo two-photon absorption within the storage medium. At a later time, another control pulse is sent, causing retrieval of the signal via stimulated emission. This memory has a number of desirable qualities. First, its use of a ladder-type level structure allows for high-bandwidth storage of the signal, as long as an appropriate broadband control pulse and one-photon detuning δ is used. Second, ORCA uses a doubly excited state for storage, which is unreachable by thermal excitation, therefore removing this as a source of noise. The ladder structure also means that four-wave-mixing noise will not be present. The use of an excited state for storage, however, will limit the maximum lifetime of the memory to that of the excited state. There will also be a reduction in the ORCA memory lifetime at room temperature due to motional-induced dephasing [18].

To date, there have been four experimental implementations of ORCA. Kaczmarek *et al.* [18] have used a cesium-filled cell for the storage medium. The D_2 line has been used, with $6S_{1/2}(F=4) \rightarrow 6P_{3/2}(F'=3,4,5)$ as the ground- to first-excited-state "signal" transition and $6P_{3/2}(F'=3,4,5) \rightarrow 6D_{5/2}(F''=2,3,4,5,6)$ as the excited- to storage-state "control" transition. These transitions have wavelengths of 852 nm and 917 nm, respectively, and the substantial difference in wavelengths results in significant motional-induced dephasing, reducing the lifetime to 5.4 ns. Kaczmarek *et al.* have also verified the preservation of single-photon statistics and the noise-free nature of the memory. Finkelstein *et al.* [17] have used a rubidium- (^{87}Rb) filled cell. Using the transitions $5S_{1/2}(F=2) \rightarrow 5P_{3/2}(F'=3) \rightarrow 5D_{5/2}(F''=4)$, with corresponding wavelengths of 780 nm for the signal and 776 nm for the control, the effect of motional-induced dephasing has been greatly reduced and a lifetime of 89 ns has been demonstrated. Since these initial works, Thomas *et al.* have demonstrated ORCA using a telecommunications wavelength for the control pulse, achieving a memory efficiency of 20%, and Davidson *et al.* have improved the scheme implemented by Finkelstein *et al.* to achieve a memory efficiency of over 50% [20].

The storage medium for all of these realizations has been composed of a warm atomic vapor contained within a glass cell. Due to beam diffraction while propagating in the cell, it is difficult to maintain a sufficiently high control-pulse intensity along the full length of the memory to enable efficient coherent excitation between the ground and storage states for the signal field. Kaczmarek *et al.* have required control fields with a peak power up to 3 W to achieve a maximum memory efficiency of 17%, while Finkelstein *et al.* have had to use up to 200 mW to achieve an efficiency of 32% and Davidson *et al.* have used a peak power of 1.4 W. These power requirements make it difficult to scale up this technology to even tens of memories, let alone the millions required for a universal quantum computer.

Guided-wave memories enable stronger coupling with lower control-power requirements. Solid-state-waveguide memories have, to date, been inefficient [21]. Another type of guided-wave memory is based on atom-loaded hollow-core photonic crystal fibers (HCPCFs), which have demonstrated significant optical absorption and phase shifts [22–25]. This makes HCPCFs a promising platform for high-efficiency quantum memories. However, due to the intricacies of using HCPCFs, only a handful of realizations have been demonstrated [14,26–29]. Of these, the only demonstration using a high-bandwidth quantum memory technique has been an implementation of Raman-type storage using a warm cesium vapor by Sprague *et al.* and this was found to be noisy at the few-photon level [14].

In this work, we demonstrate the noise-free ORCA memory protocol inside an HCPCF. This reduces the

power needed to reach the required memory efficiencies. The development of a system where the memory takes place within a fiber also lends itself to integration with optical-fiber networks. We achieve similar memory efficiencies to previous work but with a control-power reduction of 2 orders of magnitude, demonstrating that waveguides such as HCPCFs present an opportunity to increase the scalability of optical quantum memories for future large-scale optical quantum computing systems.

II. EXPERIMENT

The key components of the experimental setup were a vacuum chamber that contained the HCPCF, two external cavity diode lasers (ECDLs), and two fiber-based Mach-Zehnder interferometers (MZIs). This setup is shown in Fig. 2(a). A 30-cm length of single-cell kagome HCPCF with a core diameter of 45 μm [24] [Fig. 2(b)] was mounted in the vacuum chamber. This fiber supports an optical mode of 32.9 ± 0.6 μm, with a guidance range between 600 and 1700 nm. The vacuum chamber and fiber were filled with a Rb vapor containing a natural abundance of ^{87}Rb and ^{85}Rb. This was achieved by flooding the vacuum chamber with Rb vapor from a 1-g Rb ampoule. Over time, the Rb slowly diffuses into the core of the fiber until the vapor pressure reaches an equilibrium condition. The HCPCF being used had been under vacuum and exposed to Rb vapor for more than 5 years; thus we expected the fiber to be completely filled with Rb vapor. The chamber was heated to 80°C to increase the Rb number density in the fiber and therefore the optical depth (OD) of the system.

A 780-nm ECDL generated the signal light, which was blue detuned by 1.8 GHz from the ^{85}Rb $5S_{1/2}(F = 3) \rightarrow 5P_{3/2}(F' = 4)$ transition. This laser produced a continuous-wave (cw) output of 30 mW with a line width of less than 1 MHz, measured over 100 ms. A 776-nm ECDL generated the control light, which was tuned close to the $5P_{3/2} \rightarrow 5D_{5/2}$ transition to ensure two-photon resonance, as shown in Fig. 3. This laser produced a cw output of 90 mW. Both cw lasers were intensity modulated using

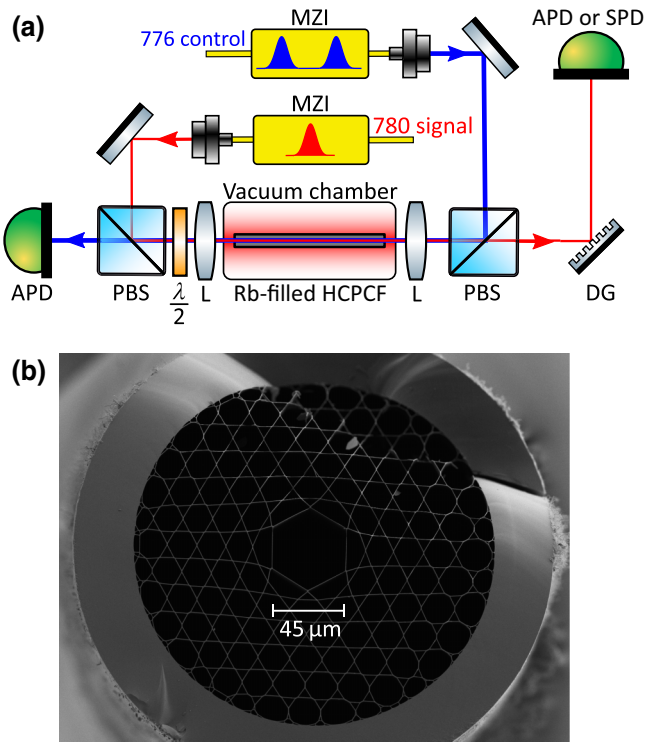

FIG. 2. The implementation of ORCA in a hollow-core photonic crystal fiber. (a) The simplified experimental setup: MZI, Mach-Zehnder interferometer; PBS, polarizing beam splitter; λ/2, half-wave plate; HCPCF, hollow-core photonic crystal fiber; DG, diffraction grating; APD, avalanche photodiode; SPD, single-photon detector; L, lens. (b) A scanning-electron-microscope image of the end face of a kagome-style HCPCF.

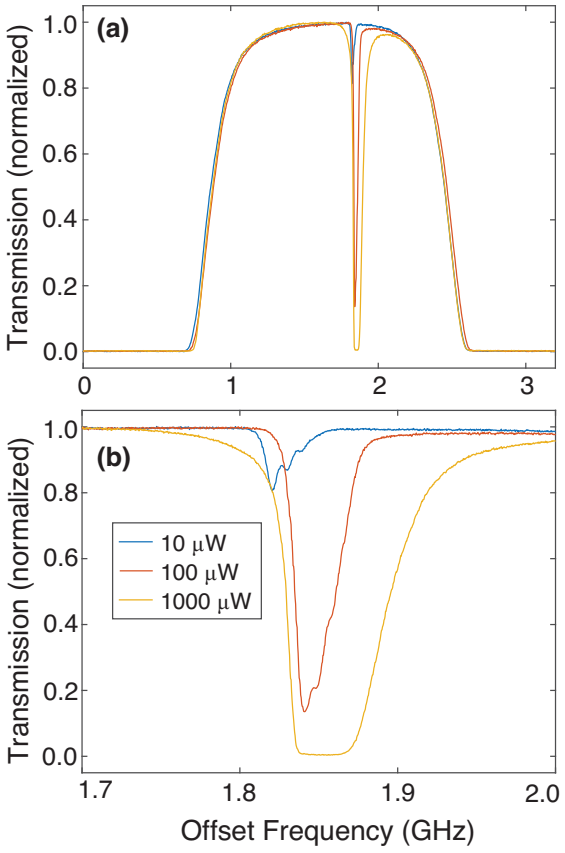

FIG. 3. Two-photon absorption. (a) The signal transmission as a function of the laser frequency offset from the ^{85}Rb $5S_{1/2}(F = 3) \rightarrow 5P_{3/2}(F' = 4)$ transition in the presence of a continuous control field with various powers (see legend). Two-photon absorption is seen at a detuning of approximately 1.8 GHz in this case, with (b) showing hyperfine details of the two-photon transition. Without the control field present, no signal absorption is seen at this offset frequency.

MZIs to create nanosecond-long pulses. The extinction ratio of the MZIs was maximized through both temperature stabilization and feedback to the bias voltage from cw power monitoring. Through this method, we were able to achieve a stable extinction ratio of order 1000:1 for both MZIs. The optical pulses produced were 4.5 ns full width at half maximum (FWHM), limited by the bandwidth of the drive electronics. Taking the Fourier transform of the optical pulse temporal profile shows a 260-MHz FWHM minimum-frequency bandwidth.

The signal and control fields were aligned into the HCPCF in a counterpropagating arrangement with orthogonal linear polarizations. After passing through the HCPCF, the two fields were separated using polarizing beam splitters (PBSs). The control field was detected using a high-bandwidth avalanche photodiode (APD). Additional filtering of the control from the signal was achieved using a diffraction grating. For relatively high signal power measurements (i.e., approximately 1 μW peak power), a high-bandwidth APD was used. For single-photon-level signal fields, the signal light was detected using a fiber-coupled single-photon-counting detector with 60% quantum efficiency. The measured collection efficiency for the single photons between the HCPCF and the single-photon detector was 5.3%, which includes losses from the diffraction grating and single-mode fiber (SMF) coupling.

Control of the pulse powers was achieved using a combination of the MZI drive voltage and neutral-density filters (NDFs). The maximum amount of light available for the control pulses was 1.47 mW through the HCPCF due to limitations on the power through the MZI and the coupling into the HCF (25%).

Figure 3(a) shows the transmission of a 1-μW cw signal field through the HCPCF in the presence of a cw pump. The frequency of the signal laser was scanned across the ^{85}Rb $5S_{1/2} \rightarrow 5P_{3/2}$ transition with the strong absorption centered at offset frequencies of approximately 0 and 3 GHz, respectively, arising from the single-photon D_2 transitions from the $F = 3$ and $F = 2$ ground states. From this scan, we calculate an OD of 74. The cw control field leads to $5S_{1/2}(F = 3) \rightarrow 5P_{3/2}(F' = 2, 3, 4) \rightarrow 5D_{5/2}(F'' = 1, 2, 3, 4, 5)$ manifold two-photon absorption approximately 1.8 GHz blue detuned from the $F = 3$ ground state. In the absence of the control field, there will be no absorption of the signal field at this offset frequency.

Figure 3(b) shows the partially resolved hyperfine structure of the two-photon transition [30] for three different powers of the control field. As can be seen, complete absorption of the signal field is possible through the HCPCF for 1-mW cw control power. At low control powers, transit-time broadening obscures the hyperfine structure, while at higher powers, the transition becomes power broadened [24].

To operate at the single-photon level, we set the average photon number per pulse $\langle N_{in} \rangle \approx 0.5$ for the signal field and used a single-photon-counting detector to measure the recalled pulses from the memory, with a system repetition rate of 100 kHz. Figure 4 shows an average of

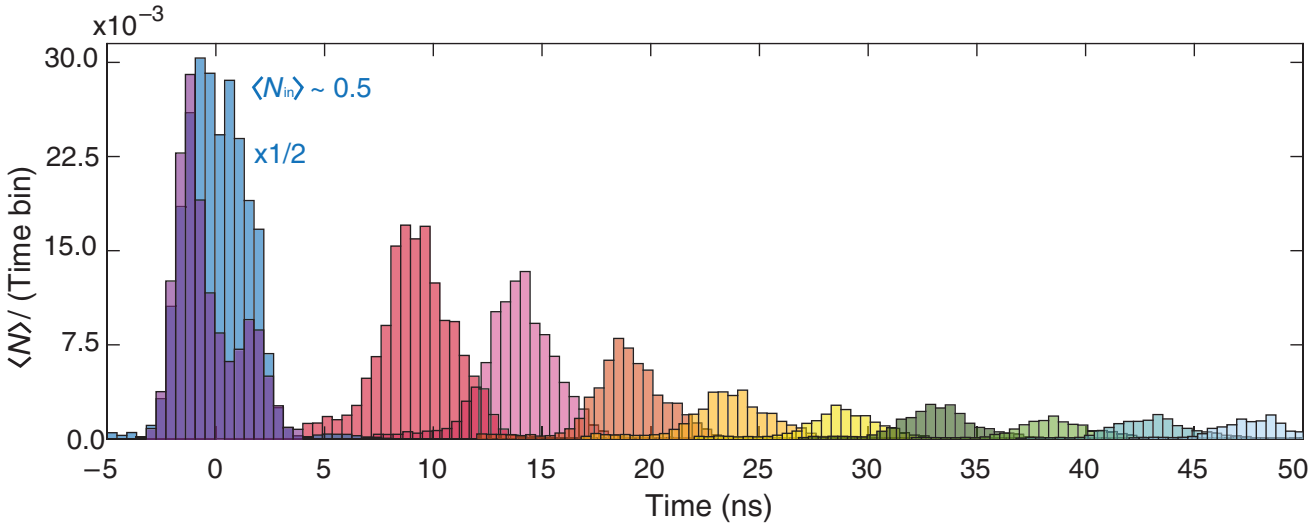

FIG. 4. The ORCA performance at the single-photon level within a rubidium-filled hollow-core photonic crystal fiber. Here, we used an average input photon number $\langle N_{in} \rangle$ of approximately 0.5 and a single-photon-counting detector. The input signal pulse with no "write" control pulse present (blue) is scaled by 0.5 to allow for easy viewing of the recall pulses. The signal leakage (i.e., the amount of signal that is not absorbed by the storage medium) is shown in purple. All other traces show the size of the signal recalled from the memory when a secondary "read" control pulse is present at different delay times. All traces are averaged over approximately 2×10^7 experimental runs, binned in 450-ps time increments, and scaled by the single-photon collection efficiency (5.3%) and the detector quantum efficiency (60%) to determine the photon number exiting the HCPCF.

approximately 2×10^7 experimental runs for the ORCA protocol inside the HCPCF for different recall times. We have scaled these results by the SMF-coupled single-photon detector quantum efficiency as well as the collection efficiency of the system. The large pulse (blue) at 0 ns is the signal pulse after passing through the system unabsorbed with no control field present. To store the signal in the memory, the "write" control and signal pulses are temporally and spatially overlapped in the fiber, causing significant absorption of the signal pulse at 0 ns (purple). To recall the stored signal pulse, a second "read" control pulse is injected into the fiber at varying delay times (other colors).

III. RESULTS

Figure 5(a) shows the efficiency of the memory for recall times from 10 ns to 40 ns using higher-photon-number probe pulses and the APD for detection for higher signal-to-noise measurements. The maximum internal efficiency measured was 28% at a 10 ns delay—the minimum delay possible with our MZI driving electronics. The use of larger probe pulses and the free-space APD removes the need to couple light into a SMF, making the external efficiency approximately 7.5% at 10-ns delay time, due to the 25% coupling efficiency of the 780-nm signal into the HCPCF, as well as losses due to the use of a diffraction grating.

The experimental decay data were fitted with an exponential decay of the form $\eta_t = \eta_0 e^{-t/\tau_s}$. From this fit, we calculate the $1/e$ memory lifetime τ_s to be approximately 10 ns. We generated a theoretical decay curve by fitting the two-photon absorption profile from Fig. 3(b) using five Voigt profiles for each of the hyperfine components and taking the fast Fourier transform (FFT) of the fit. This is represented by the dashed black line in Fig. 5(a), which predicts a lifetime of 9.54 ns. This is fully consistent with the measured value within this HCPCF, which contains both transit-time broadening and hyperfine beating effects [24]. The measured memory lifetime is roughly an order of magnitude lower than the longitudinal dephasing-limited lifetime for the Rb ORCA system [17,18], significantly limiting the fractional delay of the system to 0.7.

Another factor that could affect the observed lifetime of the system is cw leakage of both the signal and control fields through the MZIs, as this can lead to premature deexcitation of the memory. To investigate the effect of cw field leakage in more detail, we varied the extinction ratio of the control field and measured the corresponding memory lifetime. This is shown in Fig. 5(b). As can be seen, at extinction ratios below 200:1, the background control light does lead to a slight reduction of up to 20% in lifetime but above this level no adverse effect is observed.

As two-photon absorption is dependent on the control intensity, increasing the power of the control pulse should increase the efficiency of the memory. This behavior is seen for cw signals in Fig. 3(b). Figure 6(a) shows the storage efficiency (the fraction of the input signal pulse absorbed), the recall efficiency (the fraction of the absorbed signal pulse recalled), and the total efficiency (the fraction of the input signal pulse recalled) of the HCPCF ORCA system at the single-photon level as a function of the peak pulsed control power. It can be seen that the total efficiency is still increasing at the maximum control power available. At this maximum power, we achieve an internal efficiency of approximately 30%. This is the same efficiency as has been achieved in a Rb vapor cell system [17] but with a 100-fold reduction in the control power.

We then proceeded to model the system using Maxwell-Bloch equations, treating the atoms as a three-level system

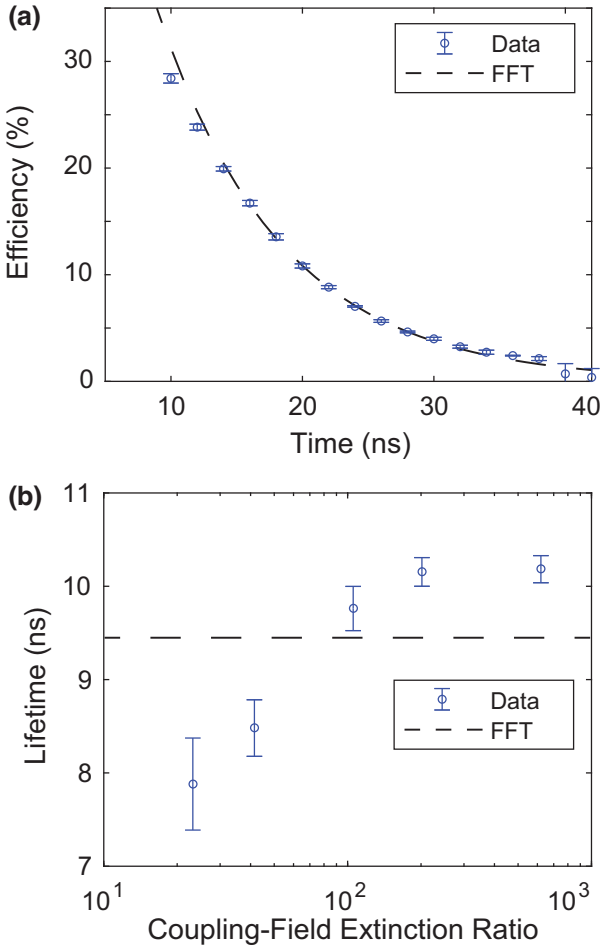

FIG. 5. The ORCA lifetime. (a) The measured efficiency of the ORCA protocol within the HCPCFs for different recall times. The dashed black line shows the predicted decay in efficiency derived from an FFT of the measured ^{85}Rb spectra. (b) The measured lifetimes of the memory for different MZI extinction ratios of the control pulses. The black line is the predicted lifetime from FFTs of the ^{85}Rb spectra from (a), not including any effects due to reduced MZI extinction ratios. The error bars indicate the standard deviation of five individual measurements.

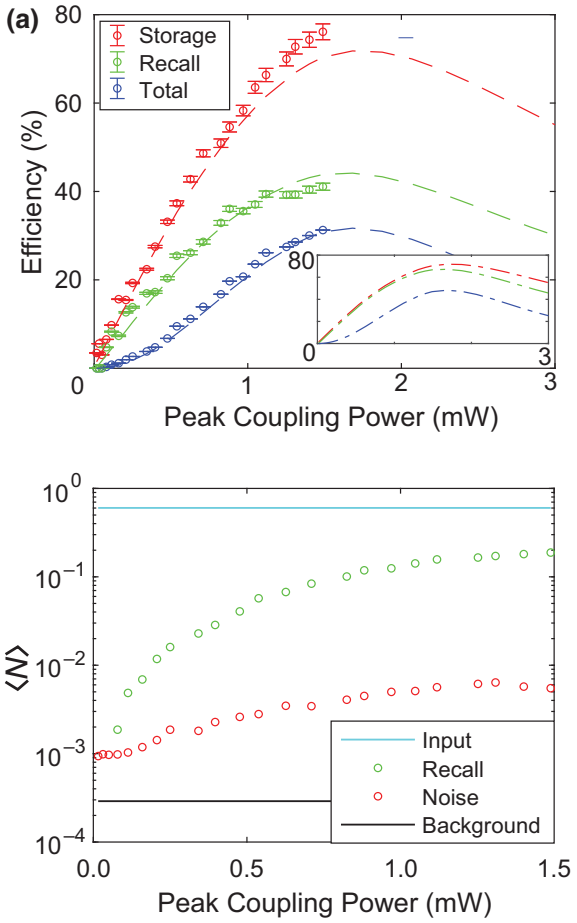

FIG. 6. The control-power effect on ORCA in the Rb-filled HCPCF. (a) The experimentally measured storage (red points) and total efficiencies (blue points) for the HCPCF ORCA system, as well as calculated recall efficiencies (green points) for a range of peak powers of the control pulses. The error bars represent the standard deviation of five typical measurement data sets. The dashed lines represent modeling of the system using a simple model with efficiency reduction due to decoherence included. The insert represents modeling with the same parameters but without decoherence. (b) The average number of signal photons per pulse for different control powers for the recalled pulse (green points) and noise (red points). Also shown are the input signal level (blue line) and the background level with both the signal and the control physically blocked (black line).

and propagation as one-dimensional with scalar fields (corresponding to fixed polarization) [31]. The model contains no free parameters, with the model OD set to the highest OD of the measured absorption spectrum. The outcome of this modeling is displayed as the solid lines in Fig. 5(a), with the excellent agreement seen vindicating this simplified model. The model does not include any decay of the stored coherence. To apply the loss related to the limited memory lifetime, the modeled retrieval efficiency was multiplied by the decay value from curve in Fig. 5(a) (dashed lines) for the storage time set in the experiment. The inset shows the model results without the rescaling (i.e., no decoherence).

The final factor to consider in terms of memory performance is the noise of the system. Figure 6(b) shows noise measurements with the system operating at the single-photon level with a 10-ns storage time. The lower limit on the noise level at 10^{-3} corresponds to the measured extinction ratio of the signal field of approximately 1000:1. The linear increasing component seen above 0.5-mW control-field power is likely due to coupling of the control light into the signal detector. This is despite the use of counterpropagating beams, orthogonal beam polarizations in conjunction with a PBS, and a diffraction grating for a total control-field extinction of approximately 100 dB. Even so, the maximum noise level is approximately a 100th of the input signal size at the single-photon level.

IV. DISCUSSION

We have demonstrated here that the use of an HCPCF can produce similar memory efficiencies to other free-space ORCA implementations but with a significantly reduced control-power requirement. While the maximum control power in the HCPCFs was limited by the damage threshold of the MZIs and the coupling efficiency into the HCPCFs, our modeling indicates that we were approaching a control power at which the total efficiency will reach a maximum, given the available OD. Additional increases in efficiency could be attained by a number of experimental elaborations. For instance, higher HCPCF chamber temperatures or light-induced atomic desorption (LIAD) can enable higher ODs for stronger light-atom interactions [32].

Pulse shaping could also be employed to achieve near-unit storage efficiency [33], using the MZIs to change the bandwidths of the control and signal, $\mathcal{B}_c$ and $\mathcal{B}_s$, respectively. The retrieval efficiency will eventually be limited by reabsorption in the atomic ensemble. This, in turn, could be removed in a scheme with backward retrieval [34]. Alternatively, full retrieval could be approached by driving the system with a higher-energy "read" pulse [35].

Our modeling shows that bandwidth matching ($\mathcal{B}_c = 1.7 \times \mathcal{B}_s$) and fine tuning the intermediate state detuning to 1.1 GHz would lead to a total efficiency, excluding decoherence, of 62% without the need to alter the experimental system. If higher control powers of up to 50 mW and increased ODs were available, the total efficiency of each node could rise to 88%. Even higher efficiencies could be achieved by appropriately shaping both the amplitude and phase of the control pulse [36].

The lifetime of ORCA within the HCPCF also limits the efficiency of the system, with modeling showing that, for an infinite lifetime memory, a maximum recall efficiency of approximately 50% would be achieved with the same

parameters as used above [Fig. 6(a) inset]. In the HCPCF system, the lifetime of the memory is greatly reduced from the motional-induced dephasing limit of 89 ns to 10 ns, predominantly due to hyperfine beating, which could be removed using optical pumping, recently demonstrated within alkali-filled HCPCFs [37].

One option to increase the memory lifetime would be to load laser-cooled atoms into the HCPCF. Quantum memory implementations using cold atoms inside HCPCFs have achieved storage times of up to 50 ms [28], orders of magnitude longer than the excited-state lifetime of 240 ns [38] and with significantly higher ODs of the order of hundreds to thousands [23,25]. However, this would greatly reduce the practicality of using such a memory in a fiber-based quantum information network.

Without the move to laser-cooled atoms, transit-time-broadening effects will mask the rephasing of the system efficiency expected at around 100 ns. A larger-diameter HCPCF would reduce the effect of transit-time broadening at the expense of reducing the memory efficiency, assuming that the maximum control power is already being used. There is, therefore, a trade-off to be made between lifetime, efficiency, and minimizing power requirements.

The noise generated by the experiment is multiple orders of magnitude above that of other ORCA realizations. This is a combination of cw leakage of the signal field through the MZIs, as well as scattering of the control field into the signal collection fiber. This could be easily improved by 14 orders of magnitude by using multiple narrower free-space band-pass filters as in other ORCA experiments [17].

To allow for greater scaling up, fiber-based solutions such as circulators and fiber Bragg gratings could be used, with single gratings being able to provide greater than 30 dB of filtering with a bandwidth of order 1 nm in the visible spectrum [39].

A key limitation on the end-to-end efficiency of the HCPCF system used here was the 25% coupling efficiency of light into the HCPCF. This efficiency is likely due to rubidium coating the inner core of the fiber. Recently, various novel methods for joining SMFs to HCPCFs have shown coupling efficiencies up to 84.5% [40] and 97% [41]. This would drastically increase the external efficiency and allow for an all-fiber quantum computing network. Alongside HCPCFs, there are a number of other optical waveguide technologies that could be used to solve scaling issues, such as antiresonant reflecting optical waveguides (ARROWs) [42] and hollow-core light cages [43]. Hollow-core light cages in particular have been three-dimensionally nanoprinted onto chips, showing their potential as easily integrated components.

Memories can be used to boost the probability of creating single photons and, crucially, photonic entangled states, for quantum computing. Taking the above-mentioned efficiency achievable with the current setup of 62% and multiplexing over sufficient temporal modes (85 possible with the Doppler-limited lifetime operating at a 1-GHz repetition rate), it would be possible to deliver on-demand single photons with 60% efficiency in fiber. Similarly, this would allow for the creation of Bell states with 35% probability and three-photon Greenberger-Horne-Zeilinger states with a probability of 11% [44,45]. Considering current laser technology, it would be possible to construct a fiber-based network of 100 ORCA memories operating at this level with an off-the-shelf 1-W amplified-ECDL system at 776 nm.

V. CONCLUSIONS

We have shown that enhancing atom-light interactions with the use of HCPCF waveguide technology can achieve the same memory efficiency as other ORCA implementations with a 100-fold reduction in pump power. While further work is required to improve the lifetime of the HCPCF memory, this work demonstrates that waveguide technologies could play a key role in the scaling up of optical quantum computing networks by allowing for efficient coupling of quantum memory systems to fiber and by significantly reducing optical power requirements for such a network of memories.

ACKNOWLEDGMENTS

B.M.S. acknowledges support from an Australian Research Council (ARC) Discovery Early Career Researcher Award (Grant No. DE170100752). J.R. acknowledges the support he has received for his research through the provision of an Australian Government Research Training Program Scholarship. The ORCA team acknowledges support from the U.S. Air Force Office of Scientific Research (AFOSR) European Office of Aerospace Research and Development (EOARD) Grant No. FA8655-21-1-7059.

[1] E. Knill, R. Laflamme, and G. J. Milburn, A scheme for efficient quantum computation with linear optics, Nature **409**, 46 (2001).

[2] S. Slussarenko and G. J. Pryde, Photonic quantum information processing: A concise review, Appl. Phys. Rev. **6**, 041303 (2019).

[3] H. J. Kimble, The quantum Internet, Nature **453**, 1023 (2008).

[4] Y. Wen, P. Zhou, Z. Xu, L. Yuan, H. Zhang, S. Wang, L. Tian, S. Li, and H. Wang, Multiplexed spin-wave-photon entanglement source using temporal multimode memories and feedforward-controlled readout, Phys. Rev. A **100**, 012342 (2019).

[5] N. Kalb, A. A. Reiserer, P. C. Humphreys, J. J. Bakermans, S. J. Kamerling, N. H. Nickerson, S. C. Benjamin, D. J. Twitchen, M. Markham, and R. Hanson, Entanglement

distillation between solid-state quantum network nodes, Science **356**, 928 (2017).
[6] Y. Pu, Y. Wu, N. Jiang, W. Chang, C. Li, S. Zhang, and L. Duan, Experimental entanglement of 25 individually accessible atomic quantum interfaces, Sci. Adv. **4**, eaar3931 (2018).
[7] J. Nunn, N. K. Langford, W. S. Kolthammer, T. F. M. Champion, M. R. Sprague, P. S. Michelberger, X. M. Jin, D. G. England, and I. A. Walmsley, Enhancing multiphoton rates with quantum memories, Phys. Rev. Lett. **110**, 133601 (2013).
[8] A. I. Lvovsky, B. C. Sanders, and W. Tittel, Optical quantum memory, Nat. Photonics **3**, 706 (2009).
[9] C. Simon *et al.* Quantum memories: A review based on the European integrated project "Qubit Applications (QAP)", Eur. Phys. J. D **58**, 1 (2010).
[10] Y.-F. Hsiao, P.-J. Tsai, H.-S. Chen, S.-X. Lin, C.-C. Hung, C.-H. Lee, Y.-H. Chen, Y.-F. Chen, I. A. Yu, and Y.-C. Chen, Highly efficient coherent optical memory based on electromagnetically induced transparency, Phys. Rev. Lett. **120**, 183602 (2018).
[11] M. Hosseini, G. Campbell, B. M. Sparkes, P. K. Lam, and B. C. Buchler, Unconditional room-temperature quantum memory, Nat. Phys. **7**, 794 (2011).
[12] S. J. Yang, X. J. Wang, X. H. Bao, and J. W. Pan, An efficient quantum light-matter interface with sub-second lifetime, Nat. Photonics **10**, 381 (2016).
[13] K. F. Reim, J. Nunn, V. O. Lorenz, B. J. Sussman, K. C. Lee, N. K. Langford, D. Jaksch, and I. A. Walmsley, Towards high-speed optical quantum memories, Nat. Photonics **4**, 218 (2010).
[14] M. R. Sprague, P. S. Michelberger, T. F. M. Champion, D. G. England, J. Nunn, X.-M. Jin, W. S. Kolthammer, A. Abdolvand, P. S. J. Russell, and I. A. Walmsley, Broadband single-photon-level memory in a hollow-core photonic crystal fibre, Nat. Photonics **8**, 287 (2014).
[15] D. G. England, K. A. G. Fisher, Jean-Philippe W. Maclean, P. J. Bustard, R. Lausten, K. J. Resch, and B. J. Sussman, Storage and retrieval of THz-bandwidth single photons using a room-temperature diamond quantum memory, Phys. Rev. Lett. **114**, 053602 (2015).
[16] P. S. Michelberger, T. F. Champion, M. R. Sprague, K. T. Kaczmarek, M. Barbieri, X. M. Jin, D. G. England, W. S. Kolthammer, D. J. Saunders, J. Nunn, and I. A. Walmsley, Interfacing GHz-bandwidth heralded single photons with a warm vapour Raman memory, New J. Phys. **17**, 043006 (2015).
[17] R. Finkelstein, E. Poem, O. Michel, O. Lahad, and O. Firstenberg, Fast, noise-free memory for photon synchronization at room temperature, Sci. Adv. **4**, eaap8598 (2018).
[18] K. T. Kaczmarek, P. M. Ledingham, B. Brecht, S. E. Thomas, G. S. Thekkadath, O. Lazo-Arjona, J. H. D. Munns, E. Poem, A. Feizpour, D. J. Saunders, J. Nunn, and I. A. Walmsley, High-speed noise-free optical quantum memory, Phys. Rev. A **97**, 042316 (2018).
[19] S. E. Thomas, S. Sagona-Stophel, Z. Schofield, I. A. Walmsley, and P. M. Ledingham, Single-photon-compatible telecommunications-band quantum memory in a hot atomic gas, Phys. Rev. Appl. **19**, L031005 (2023).
[20] O. Davidson, O. Yogev, E. Poem, and O. Firstenberg, Fast, noise-free atomic optical memory with 35-percent end-to-end efficiency, Commun. Phys. **6**, 131 (2023).
[21] J. Jin, E. Saglamyurek, Marcel li Grimau Puigibert, V. Verma, F. Marsili, S. W. Nam, D. Oblak, and W. Tittel, *et al.*, Telecom-wavelength atomic quantum memory in optical fiber for heralded polarization qubits, Phys. Rev. Lett. **115**, 140501 (2015).
[22] M. R. Sprague, D. G. England, A. Abdolvand, J. Nunn, X. M. Jin, W. Steven Kolthammer, M. Barbieri, B. Rigal, P. S. Michelberger, T. F. Champion, P. S. J. Russell, and I. A. Walmsley, Efficient optical pumping and high optical depth in a hollow-core photonic-crystal fibre for a broadband quantum memory, New J. Phys. **15**, 055013 (2013).
[23] F. Blatt, T. Halfmann, and T. Peters, One-dimensional ultracold medium of extreme optical depth, Opt. Lett. **39**, 446 (2014).
[24] C. Perrella, P. S. Light, S. A. Vahid, F. Benabid, and A. N. Luiten, Engineering photon-photon interactions within rubidium-filled waveguides, Phys. Rev. Appl. **9**, 044001 (2018).
[25] A. P. Hilton, C. Perrella, F. Benabid, B. M. Sparkes, A. N. Luiten, and P. S. Light, High-efficiency cold-atom transport into a waveguide trap, Phys. Rev. Appl. **10**, 044034 (2018).
[26] F. Blatt, L. S. Simeonov, T. Halfmann, and T. Peters, Stationary light pulses and narrowband light storage in a laser-cooled ensemble loaded into a hollow-core fiber, Phys. Rev. A **94**, 043833 (2016).
[27] W. Li, P. Islam, and P. Windpassinger, Controlled transport of stored light, Phys. Rev. Lett. **125**, 150501 (2020).
[28] W. S. Leong, M. Xin, C. Huang, Z. Chen, and S.-Y. Lan, Long light storage time in an optical fiber, Phys. Rev. Res. **2**, 033320 (2020).
[29] T. Peters, T.-P. Wang, A. Neumann, L. S. Simeonov, and T. Halfmann, Single-photon-level narrowband memory in a hollow-core photonic bandgap fiber, Opt. Express **28**, 5340 (2020).
[30] F. Nez, F. Biraben, R. Felder, and Y. Millerioux, Optical frequency determination of the hyperfine components of the two-photon transitions in rubidium, Opt. Commun. **102**, 432 (1993).
[31] K. T. Kaczmarek, Ph.D. thesis, University of Oxford, Clarendon Laboratory (2017).
[32] K. T. Kaczmarek, D. J. Saunders, M. R. Sprague, W. S. Kolthammer, A. Feizpour, P. M. Ledingham, B. Brecht, E. Poem, I. A. Walmsley, and J. Nunn, Ultrahigh and persistent optical depths of caesium in kagome-type hollow-core photonic crystal fibres, Opt. Lett. **40**, 5582 (2015).
[33] I. Novikova, N. B. Phillips, and A. V. Gorshkov, Optimal light storage with full pulse-shape control, Phys. Rev. A **78**, 021802(R) (2008).
[34] A. V. Gorshkov, A. André, M. Fleischhauer, A. S. Sørensen, and M. D. Lukin, Universal approach to optimal photon storage in atomic media, Phys. Rev. Lett. **98**, 123601 (2007).
[35] J. Nunn, I. A. Walmsley, M. G. Raymer, K. Surmacz, F. C. Waldermann, Z. Wang, and D. Jaksch, Mapping broadband single-photon wave packets into an atomic memory, Phys. Rev. A **75**, 011401(R) (2007).

[36] J. Guo, X. Feng, P. Yang, Z. Yu, L. Chen, C.-H. Yuan, and W. Zhang, High-performance Raman quantum memory with optimal control in room temperature atoms, Nat. Commun. **10**, 148 (2019).

[37] T. Krehlik, A. Stabrawa, R. Gartman, K. T. Kaczmarek, R. Löw, and A. Wojciechowski, Zeeman optical pumping of ^{87}Rb atoms in a hollow-core photonic crystal fiber, Opt. Lett. **47**, 5731 (2022).

[38] D. Sheng, A. Pérez Galván, and L. A. Orozco, Lifetime measurements of the 5*d* states of rubidium, Phys. Rev. A **78**, 062506 (2008).

[39] M. Becker, T. Elsmann, A. Schwuchow, M. Rothhardt, S. Dochow, and H. Bartelt, Fiber bragg gratings in the visible spectral range with ultraviolet femtosecond laser inscription, IEEE Photonics Technol. Lett. **26**, 1653 (2014).

[40] D. Fan, Z. Jin, G. Wang, F. Xu, Y. Lu, D. J. J. Hu, L. Wei, P. Shum, and X. Zhang, Extremely high-efficiency coupling method for hollow-core photonic crystal fiber, IEEE Photonics J. **9**, 7104108 (2017).

[41] D. Suslov, M. Komanec, E. R. Numkam Fokoua, D. Dousek, A. Zhong, S. Zvánovec, T. D. Bradley, F. Poletti, D. J. Richardson, and R. Slavík, Low loss and high performance interconnection between standard single-mode fiber and antiresonant hollow-core fiber, Sci. Rep. **11**, 8799 (2021).

[42] B. Wu, J. Hulbert, A. Hawkins, and H. Schmidt, Planar hollow-core waveguide technology for atomic spectroscopy and quantum interference in alkali vapors, J. Lightwave Technol. **26**, 3727 (2008).

[43] C. Jain, A. Braun, J. Gargiulo, B. Jang, G. Li, H. Lehmann, S. A. Maier, and M. A. Schmidt, Hollow core light cage: Trapping light behind bars, ACS Photonics **6**, 649 (2019).

[44] M. Varnava, D. E. Browne, and T. Rudolph, How good must single photon sources and detectors be for efficient linear optical quantum computation?, Phys. Rev. Lett. **100**, 060502 (2008).

[45] S. Bartolucci, P. M. Birchall, M. Gimeno-Segovia, E. Johnston, K. Kieling, M. Pant, T. Rudolph, J. Smith, C. Sparrow, and M. D. Vidrighin, Creation of entangled photonic states using linear optics, Preprint ArXiv:2106.13825v1 (2021).